UDC 539.1.06, 544.022.6, 544.022.51

X-ray Absorption Spectroscopy as a Tool for Studying and Developing Novel Materials

D. I. KOCHUBEY and V. V. KANAZHEVSKII

Boreskov Institute of Catalysis, Siberian Branch of the Russian Academy of Sciences, Pr. Akademika Lavrentyeva 5, Novosibirsk 630090 (Russia)

E-mail: kochubey@catalysis.ru

Abstract

Despite the abundance of available experimental techniques, the X-ray absorption spectroscopy often remains the only acceptable means for solving a number of problems: studying X-ray amorphous substances, determining the phase composition at a lower concentration limit for impurity samples, determining the valence state of a chemical element in the case of a low content thereof in the sample (mass percent quota). The present review reports the theory and examples of successful applying the methods of EXAFS and XANES to solve complicated problems.

Key words: EXAFS, XANES, X-ray absorption spectroscopy, platinum nanoparticles, gold nanoparticles, molybdenum sulphate, zirconium oxychloride in the sulphuric acid, cobalt valence state in compounds, ruthenium-rubidium catalysts

Table of contents

INTRODUCTION

In the course of developing novel materials or in the case of serial production thereof it is required to determine the materials' physical and chemical parameters. This requirement could be also applied to nanomaterials, but in this case to apply the methods developed earlier is often not possible. In particular, the traditional X-ray based methods are not suitable for the investigation of nanomaterials with the characteristic size less than 100–10 nm because

of so-called X-ray amorphism thereof (though in reality they have a crystalline structure). In order to determine the structure of these materials and the phase composition of the constituent components, within the last 30 years one uses the method of X-ray absorption spectroscopy (EXAFS spectroscopy).

The determination of the valence state for the elements those constitute the nanomaterials (primarily nanocomposites) could also be problematic because of a low content of the elements under investigation in the material. Measuring the valence state using X-ray photoelectron spectroscopy is possible usually when the concentration of the element under investigation is not less than several atomic percent. Currently, this problem is solved also by means of using the X-ray absorption spectroscopy, but in a slightly different manner as to compare with the EXAFS spectroscopy (so-called XANES spectroscopy).

In the course of the investigation of multiphase composite nanomaterials, the determination of the phase composition could be complicated, even in the case of materials involving well-crystallized phases, because of a great number of phases or a low content of the phase under investigation. The traditional X-ray diffraction methods allow performing the phase analysis for not more than five phases contained in the object under investigation, when the phase content is greater than 5 %.

It is well known [1–3] that the energy position of the extended fine structure (EFS) features in X-ray absorption spectra (XAS) is determined, primarily, by the nature and arrangement geometry of the atoms of the nearest surrounding with respect to an absorbing atom. The first theoretical explanation of the EXAFS (Extended X-ray Absorption Fine Structure) nature was presented by the authors of [4]. Further, the theory of EXAFS was considered by the authors of [5–7]. A great contribution to the development of the theory made by Soviet scientists. So, in the 1940s, the authors of [8, 9] made a significant development of the EXAFS theory. A further important step was taken by the authors of [10–13] in 1960. Nowadays, great interest in the EXAFS, both from the standpoint of practical application, and within the framework of further developing the theoretical description for the mechanisms of the formation of X-ray spectrum far from the beginning of the absorption edge, was reflected in papers [14–16]. Their authors have convincingly demonstrated that the study of X-ray spectra of EFS is not only interesting from the spectroscopic point of view, but also they can be used in order to study the structure of the nearest environment of the absorbing atom.

THEORY OF EXAFS SPECTROSCOPY

X-ray absorption by matter

The attenuation of X-ray radiation intensity with the wavelength amounting to about 1–10 Å in a substance containing atoms with mediate atomic numbers (Z ~ 15–40), is caused by a so-called true X-ray absorption [1]. The dependence the intensity of radiation passing the distance (x) through the matter with the atomic mass (A) and density (ρ), depending on the incident radiation intensity (for an area equal to 1 cm^2) can be described in the general form as

$$\frac{I_x}{I_0} = \exp\left(-\mu_m m\right) = \exp\left(-\mu_a \frac{\rho N_A}{A} x\right)$$

where m is the mass of the material wherethrough the radiation passes; N_A is the Avogadro's number; μ_m is the mass absorption coefficient, usually observed in experiments; μ_a is the atomic absorption coefficient. In fact, the atomic absorption coefficient represents an area of the effective cross section of the atom for X-ray absorption [1]. It can be considered as a sum of the atomic absorption coefficients (μ_q) inherent in corresponding atomic energy levels.

According to the theory of X-ray based methods, the energy levels are indicated as it follows: K – $1s$ ($^2S_{1/2}$), L_I – $2s$ ($^2S_{1/2}$), L_{II} – $2p$ ($^2P_{1/2}$), L_{III} – $2p$ ($^2P_{3/2}$), M_I – $3s$ ($^2S_{1/2}$) and so on. Corresponding transitions caused by the ionization of electrons from the mentioned levels are indicated in a similar manner.

The atomic coefficient depends on the nature of an absorbing atom (Z) and on the wavelength (λ) of the radiation absorbed [1]:

$m_q \sim C(\lambda_q)Z^4\lambda^3$

where C is a coefficient which depends on the wavelength and changes with going through λ_K, λ_L, λ_M values and so on corresponding to

the wavelength values those cause the ionization of certain energy levels. It is known that with increasing the parameter of λ the absorption coefficient exhibits a monotonous increase, and when $\lambda = \lambda_q$ it decreases abruptly. The latter fact is caused by the absorption jump due to the ionization of the electronic level. Such jumps are called absorption edges.

Photoelectron scattering

The X-ray absorption coefficient (μ_q) could be calculated using well-known formula for atomic absorption [17, 18]:

$$\mu_q = 4N_0\pi^2 l^2 \left(\frac{\varpi}{c}\right) \left|\langle \psi_j | z | \psi_q \rangle\right|^2 \rho(T)$$

where N_0 is the number of atoms per unit volume of the material; ψ_j, ψ_q are the wave functions of the final and initial states of the photoelectron, respectively; ω is the frequency of the absorbed X-ray photon; $\rho(T)$ is the density of final states.

The m_q value for certain energy $T = h\nu - E_q$ (E_q is the energy of level q) should depend on the nature of the final state wave function near the absorbing atom, since this is just the area wherein the wave function of the initial state is localized. Consequently, the value of the matrix element $|...|^2$ is determined by the value of wave function ψ_j within the localization region of the wave function of the initial state ψ_q (coinciding, for example, with 1*s* function in the case of *K* edge absorption).

The amplitude of the ψ_j function within either area of a molecule or a crystal is affected by the interference of primary and scattered waves (Fig. 1). Just changing the μ_q value depending on the energy of the ejected electron (T) causes the extended X-ray absorption fine structure (EXAFS) far from the absorption edge (outside the range of 10 eV, called XANES *i. e.* X-ray Absorption Near Edge Structure).

The interference effects of the interaction between the primary and reflected waves are determined, first of all, by a mutual arrangement of the atoms that emitted photoelectron, and the atoms those are involved in the scattering. It is obvious that the reflection of the electron wave from the surrounding atoms should depend on the nature of the latter. Just these features of EXAFS can be used to study the geometry of the short-range order for a wide class of objects; including the objects, those are not simple for the most of structural methods such as highly dispersed catalysts or catalysts with a low content of the component under investigation (hundredths of percent).

The main features of EXAFS spectra consist in the modulations caused by changing the matrix element of monotone (outside the absorption edge) $\rho(T)$ function. The fine structure of X-ray absorption coefficient really observed on the experimental curves represents a sum of the contributions from the oscillation of atoms located at different distances from the atom that absorbed an X-ray quantum (Fig. 2).

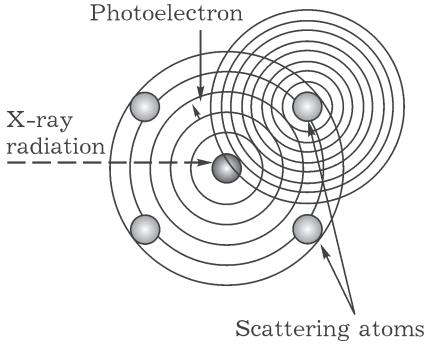

Fig. 1. Schematic diagram of photoelectron scattering on the nearest neighbours of the atom absorbing an X-ray photon.

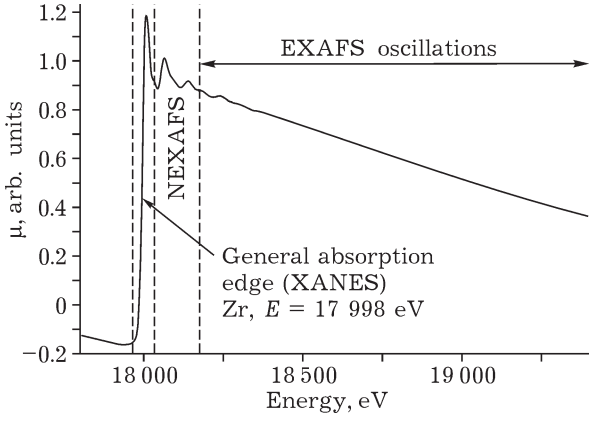

Fig. 2. Absorption spectrum of the *K* edge of zirconia (zirconium oxide cubic modification).

Technique for the isolation of EXAFS spectra

The extended X-ray absorption fine structure $\chi(k)$ (in practice, EXAFS spectroscopy predominantly uses the terms of wave vectors, rather than those of wave numbers) is determined by the following expression:

$$\chi(k) = \mu(k) - \mu_0(k)/[\mu_0(k) - \mu_1(k)]$$

where k is the modulus of photoelectron wave vector; $\mu(k)$ is experimentally obtained absorption coefficient for the sample under investigation; $\mu_1(k)$ is the absorption coefficient determined by all the processes, except for the photoionization of the atomic electron shell under investigation (the ionization of higher-level electrons, the ionization of other chemical elements, scattering); $\mu_0(k)$ is the absorption coefficient observed in the absence of neighbouring atoms near the absorbing atom. The procedure of isolating the EXAFS oscillations is demonstrated in Fig. 3.

The photoelectron wave vector is specified by relationship

$$k = \left(\frac{2m_e(h\nu - E_0)}{\hbar^2} \right)^{1/2}$$

where $h\nu$ is the energy of incident X-ray quants; E_0 is the ionization potential in the course of X-ray photon absorption; $\hbar$ is the Planck's constant. In order to construct the $\mu_1(h\nu)$ function, the pre-edge part of the absorption spectrum $\mu(h\nu)$ with $h\nu < E_0$ is extrapolated to the range of $h\nu > E_0$. In this case $\mu_1(h\nu)$ is determined by means of the method of least squares in the form of Victorin polynomials: $C(h\nu)^{-3} + D(h\nu)^{-4}$. The smooth part of the absorption coefficient $\mu(h\nu)$ is calculated using cubic splines (third degree polynomials). As a starting point E_0, that determines the point on the experimental spectrum corresponding to photoelectrons with $k = 0$, is specified by the inflection point on the edge of the absorption spectrum, which point corresponds to the position of the maximum of the first derivative of $\mu(k)$.

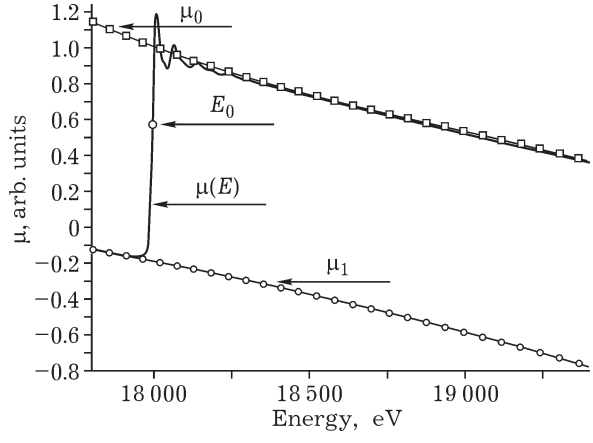

Fig. 3. Approximation of the pre-edge region and of the area beneath the *K* edge of zirconium (zirconium oxide, cubic modification).

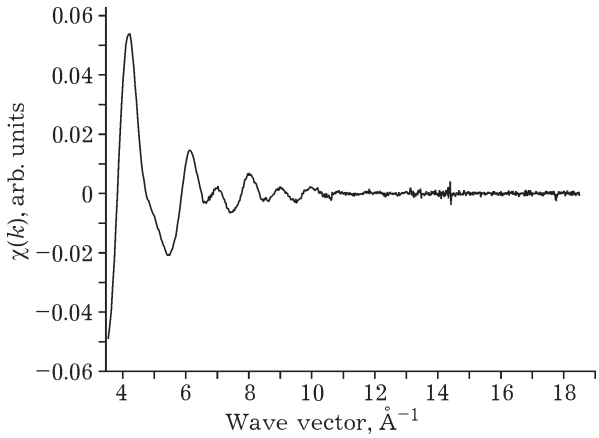

Fig. 4. Extended fine structure of X-ray absorption *K* edge of zirconium (zirconium oxide, cubic modification).

Owing to the normalization of the absorption coefficient, $\chi(k)$ becomes a function of the absorption for one atom (Fig. 4). The normalization is performed by means of dividing the value of the absorption coefficient by the value of the absorption jump at the edge: $\mu_0(k) - \mu_1(k)$.

Technique for determining the structural characteristics

It is known that the EXAFS oscillations in a single-electron approximation with taking into account single scattering are described by the formula [19]

$$\chi(k) = \frac{1}{k} \sum_i \frac{N_i F_i(k)}{R_i^2} \exp(-2\sigma_i^2 k^2) \sin\left(2kR_i + \varphi_i(k)\right)$$

where the subscript i refers to the coordination sphere of the atoms of the same type; R_i is the distance to the i-th sphere; N_i is the number of atoms of the mentioned type; σ_i is the Debye–Waller factor (structural disordering and thermal vibrations of atoms); $F_i(k)$ is the prob-

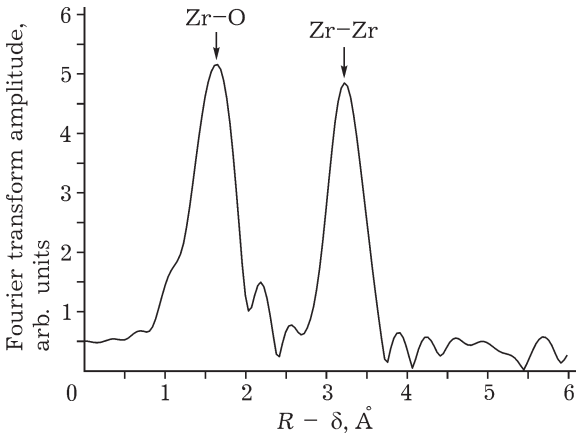

Fig. 5. Radial distribution function (cubic zirconia modification).

ability amplitude for photoelectron scattering at 180 deg (backscattering factor); $\varphi_i(k)$ is the phase change for the photoelectron occurring with emitting thereof by the central atom and backscattering.

The curve of the radial atomic distribution (RAD) $\rho(R)$ allows one to better visualize the spatial and quantitative composition of the nearest environment of an absorbing atom (Fig. 5). The quantity $\rho(R)$ is determined from the function $g(R)$, obtained basing on Fourier transform $\chi(k)$:

$$g(R) = \int_{k_{\min}}^{k_{\max}} \chi(k) k^n e^{-2ikR} dk$$

where $k_{\max}$ and $k_{\min}$ determine the interval wherein is the analysis of experimental data is performed. Factor k^n is introduced in order to compensate decreasing the χ value with increasing k ($n = 1–3$).

For further analysis, a power function of the Fourier transform is used:

$\rho(R) = \{[\mathrm{Re}(g(R))]^2 + [\mathrm{Im}(g(R))]^2\}^{1/2}$

where Re represents the real part and Im being the imaginary part of the function $g(R)$.

To obtain the most accurate structural information, researchers use a method for modelling $\chi(k)$, in particular *via* adjusting the parameters of R_i, N_i, s_i and E_0. In this case it is assumed that the chemical nature of the scattering atoms is known whereas the functions of $F_i(k)$, and $\varphi_i(k)$ are calculated theoretically for a structure proposed for the nearest environment of the absorbing atom. According to these data, $\chi_{\mathrm{mod}}(k)$ is plotted and $\|\chi(k) - \chi_{\mathrm{mod}}(k)\|$ difference is minimized (Fig. 6).

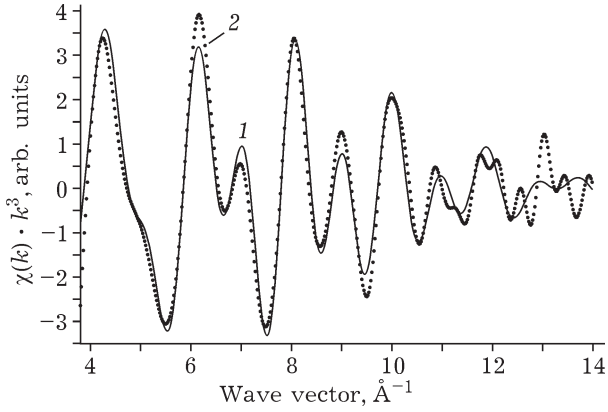

Fig. 6. $\chi(k) \cdot k^3$ and $\chi_{\mathrm{mod}}(k) \cdot k^3$ curves (zirconia, cubic modification): *1* – model, *2* – experiment.

FEATURES OF EXAFS EXPERIMENTAL TECHNIQUES

X-ray source

The most part of the outstanding results of modern science obtained using X-ray diffraction methods were achieved through the use of synchrotron radiation, *i. e.* the radiation produced by the movement of high-energy charged particles (electrons or positrons) in a magnetic field [20]. The EXAFS spectroscopy method did not become an exception, too. The main advantages of the synchrotron radiation as to compare with other X-ray sources could be considered to consist in a continuous generation; a small divergence, whereby it is easy to obtain a high intensity of radiation, spectrum extensity and the absence of any features therein.

The EXAFS Station of the Siberian Centre for Synchrotron and Terahertz Radiation uses synchrotron radiation (SR) generated by VEPP-3 storage unit (Budker Institute of Nuclear Physics, Novosibirsk). The storage unit represents a ring-type accelerator with colliding electron-positron beams. Just the powerful bending magnets of mentioned accelerator operating in the mode of storing the electrons cause the SR to occur.

The Siberian Centre for Synchrotron and Terahertz Radiation is not the only one in Russia and in the world. There are similar centres in Russia (Moscow), Germany, Italy, France,

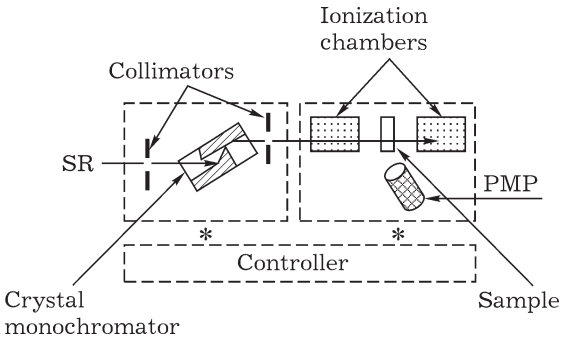

Fig. 7. Schematic diagram of an EXAFS spectrometer.

Sweden, Great Britain, India, Japan, the USA and others. In addition to the generation of the SR by the bending magnets, there are other technologies known using the wigglers, undulators, optical and X-ray klystrons, as well as combinations thereof [19].

Spectrometer arrangement

The EXAFS spectrometer consists of three main parts (Fig. 7): unit for the generation of radiation (monochromator for SR generated by VEPP-3), signal registration unit (ionization chambers in conjunction with a photomultiplier (PMP) or a solid state detector) and a controlling unit (personal computer and other electronics).

Monochromator. The radiation from the bending magnet of the VEPP-3 storage ring first of all enters an input collimator that cuts out a part of the beam corresponding to the receiving angle of the monochromator. The monochromatization of SR occurs owing to the Bragg diffraction on the single crystal surface. The spectrometer includes a double-crystal monochromator made according to a (+, −) scheme, wherein the X-ray beam monochromatized after the first reflection is reflected again by a second plane of the crystal monochromator positioned parallel to the first one. It represents a unit, wherein a pair of monochromator planes is made of a single crystal (a saw cut being made along the (111) plane of a single crystal silicon).

In this case both working planes are always rigidly connected to each other, whereby one can rotate the entire unit as a whole. The rotation of the unit is performed using a goniometer, which provides scanning the X-ray energy requires for obtaining the spectra. In our spectrometer we use an incremental scanning: after turning the crystal monochromator, a registration system is activated and signal accumulation occurs, and then the cycle is repeated. The rotation angle in one step provides an energy scanning increment approximately equal to 1−2 eV.

The output collimator provides the selection of the reflex used as the working one from the entire set of reflections from the single crystal plane.

Registering part. The most common EXAFS method is currently considered to consist in registering the spectra in a transmission mode. The standard scheme of two-beam spectrometer involves simultaneously measuring the intensity of the incident radiation (I_0) and radiation (I) transmitted through the sample. The absorption coefficient (μ) is determined as $\ln (I_0/I)$.

As the detectors proportional ionization chambers are used [23]. To measure the intensity of the incident beam and the beam transmitted through the sample a transit time chamber and a complete absorption chamber are used, respectively. Different absorption coefficients for the chambers are achieved by choosing a mixture of gases and pressure wherewith the gas mixtures are injected.

At the measurement error of current strength values in the ionization chambers $\Delta I/I \sim 10^{-4}$ the absorption coefficient error is less than 0.1 % with the absorption coefficient jump at the edge being less than 0.1−0.2 abs. units. This could be achieved through properly preparing the samples. The other errors inherent in the transmission technique is associated with a finite value of the energy resolution of the monochromator, with the presence of higher order reflection harmonics in the radiation source spectrum with the wavelength equal to $\lambda/2$, $\lambda/3$ and so on, as well as with the sample inhomogeneity.

There are other known registration methods for EXAFS spectra, for example, *via* detecting the X-ray fluorescence. In this case, instead of the ionization chamber detecting the transmitted radiation, a photomultiplier tube (PMT) or a solid state detector are used those detect the fluorescence of the sample. The fluorescence, in turn, arises in the process of electron relaxation from the upper electronic energy levels to the level ionized by X-ray radiation.

TABLE 1

Main characteristics of an EXAFS spectrometer

Parameters	Values
Storage parameters:	
electron energy	2 GeV
operating current	50–120 mA
lifetime of X-ray beam	up to 12 h and more
Main characteristics of the station:	
split crystal monochromator Si (111), energy resolution	6000
working step	0.4 ang. s
working range of X-ray energy	4.5–31 keV
measurement error for the coefficient of radiation absorption	less than 0.1 %
Chemical elements under investigation	beginning from Ti
Concentrations elements under investigation	0.01–100 mass %
Range of interatomic distances to measure	1.5–6 Å (±1 %)
Error in determining the coordination number	±10 %
Error in determining the Debye–Waller factor	±40 %

The techniques for registering the transmission and for registering the fluorescence exhibit their own advantages and limitations. The main advantage of the transmission technique consists in a high signal/noise ratio, registered for the main amount of experimental data. It is obvious that in using this technique the samples under investigation should exhibit sufficient transparency with respect to the radiation as well as the concentration of the components required for the registration of the above mentioned absorption jump value.

In the case of registering the X-ray fluorescence, the class of samples under investigation is somewhat wider; there are no requirements for the transmittance of the sample under investigation with respect to X-ray radiation, whereas the lower limit of concentrations is significantly lower than it is in the case of the transmission technique. However, there are some limitations observed, too. So, the signal/noise ratio in the course fluorescence detection is to a considerable extent less than that in the case of registering of the transmittance spectra, therefore the statistics collected at each point required for registering high-quality spectra should be substantially greater, which causes increasing the acquisition time. There could be also difficulties with samples placed in either shell, since the escape depth for the X-ray fluorescence is limited. The main characteristics of the spectrometer and the errors in determining the structural characteristics of the samples under study are presented in Table 1.

Obtaining the experimental data

The procedure for obtaining experimental data involves several stages:

1) Preparing the samples for the experiment (the calculation of concentration values and linear dimensions);

2) Controlling the experiment (adjusting for the absorption edge, setting the parameters of registration);

3) Spectra processing (the calculation of phases and amplitudes, the separation of $\chi(k)$ function, modelling the spectra).

Sample preparation

The main demand made with respect to the samples under investigation consists in the homogeneity (*i. e.* a uniform distribution of all the components over the bulk of the sample) within the area of interaction with radiation. For the majority of gaseous, liquid and gel-like samples the mentioned requirement is met due to natural causes. There is also a class of solid

samples, whose homogeneity is not questioned, such as a metal foil or polymeric materials. For the preparation of solid (crystalline or amorphous), inhomogeneous samples one need to make additional efforts. For example, the homogeneity of the samples could be achieved by means of grinding (if it does not affect the properties under consideration) with placing in plastic inert filler. Single crystals might be acted in a different manner, for example, to rotate with a sufficient angular velocity for an isotropic distribution of reflections within the scanning time of the absorption coefficient.

As previously mentioned, the most accurate results when registering EXAFS spectra can be achieved using the transmission technique. The requirements for the mentioned scheme of the experiment are relatively simple. It is necessary that the sample transmit the X-ray radiation in an amount sufficient for registering by the complete absorption chamber. Otherwise one needs to use another registration method. It is also necessary that the amount of radiation absorbed by the sample is able to provide a jump of parameter μ. It follows from this that there are optimum (and limiting) quantitative characteristics of the sample. For the calculation thereof researchers use such software as, for example, XAFSmass [24].

The EXAFS method allows the researchers to investigate a very wide class of systems. However, alongside with the conditions necessary to produce quality spectra, there are conditions for the storage of the samples (inert atmosphere or low temperature) or those for performing *in situ* studies (high temperature or an adsorption unit), which might be contrary to the conditions of the experiments. For example, the EXAFS oscillations of some elements are substantially contributed by the factor of heat (Debye–Waller factor), which complicates the extraction of information concerning the structure of the sample from the spectral data. However, this complication could be avoided in case the sample is placed in a cryostat in the course of experiment.

Spectrometer control and registering the spectra

In order to obtain a quality spectra, after calculating the concentration and linear dimension of the sample under investigation (that is usually placed in a special cell, depending on the task), researchers should provide the energy range wherein the spectrum is registered. The pre-edge region should be sufficiently long (typically 0.2–0.5 keV), so that basing on it one could extrapolate the value of μ_1. Beneath the absorption edge, one also need to register a sufficient number of points (typically 1.5–2 keV) in order to have the structural information concerning the heavier and farer neighbours of the absorbing atom. It should be noted that sometimes the absorption edge of the other elements present in the sample could be close in the energy magnitude to the energy values of EXAFS oscillations inherent in the element under observation. In the case when this phenomenon interferes with the extraction of structural information, it is necessary to use filters or narrower energy ranges.

At the stage of registering EXAFS spectrum one should take care of signal/noise ratio. At each point, it should be gained a sufficient statistics (not less than 10^6 pulses per point). For this purpose, as a rule, there are scan time values μ and the number(a mean value) for a preset energy value. It is necessary to consider that the ratio required has its own limit, whereas the registration time of the spectrum increases in proportion to the number of measurements and scanning time. In this connection it is advisable to use compromise settings, in particular, when the sample parameters or the process under investigation depend on time.

Calculation of amplitude and phase values

As previously mentioned, function $F_i(k)$, and $\varphi_i(k)$ are calculated theoretically for the proposed structure of the nearer environment of the absorbing atom. To do this there should be a countable number of hypotheses concerning an approximate geometry and composition of the local structure for the sample under investigation, those would be tested in the course of extracting the structural information.

In constructing the hypotheses researchers follow data obtained from other methods, results from studying similar systems, general laws, certain assumptions and so on. For this purpose, structural databases are quite useful, such as ICSD (Inorganic Crystal Structure Da-

tabase). Such databases usually contain data required for not only putting forward and checking the consistency of the proposed hypotheses, but there are also accurate data required for the theoretical calculation of scattering amplitudes and phases. Among them, there are space symmetry group and the sets atomic coordinates, those serve as input data for the calculation software packages. One of the most popular programs is presented by FEFF [25]. There are also software packages known those combine the calculation of phases and amplitudes with the simulation of the experimental spectra, such as EXCURVE.

Modelling the experimental spectra

It should be noted that modelling is performed directly with respect to EXAFS oscillations, in other words, the function $\chi(k)$ (see p. 18). This function was defined earlier (see p. 16); the procedure of obtaining thereof from the experimental dependence of $\mu(E)$ (so-called pre-processing) is described in detail (see Fig. 2); it is implemented in the most of software products. One of the products is presented by VIPER (Visual Processing in EXAFS Researches) [26] that includes the most of the necessary means for the visualization and direct simulation of experimental spectra using the phases and amplitudes calculated with the help of a FEFF program.

The pre-processing stage is followed by the stage of visualizing the structural information. As noted above, a RAD function is more pictorial, which function is obtained by means of the Fourier transform of the original data (see Fig. 5). Thus, for the distances corresponding to the distance between neighbouring atoms and the central (absorbing) atom, the RAD curve exhibits maxima whose amplitude is proportional to the coordination number (the number of neighbouring atoms). The width of the peaks contains information about the Debye–Waller factors.

Shift δ (see Fig. 5) represents a correction between real distances and those resulting from the Fourier transform. This value is specific for each element; it varies from one coordination sphere to another and it is associated with the presence of a linear term in the approximation dependence of the trial function. This disadvantage of the RAD curve is compensated by precise distance values obtained in the course of simulation.

Since the Fourier transform of the harmonic functions is conducted for a finite interval of wave numbers, the RAD curve alongside with the main peaks exhibit side peaks, those do not contain any structural information (see Fig. 5). One could determine the type of the maximum (real peak or side peak) *via* changing the Fourier transform range. In contrast to side maxima, the real peaks should not move.

Typically, the function $\chi(k)$ is multiplied not only by the power factor of the wave vector, as previously mentioned, but also by a function smoothing the edges of the Fourier transform range. The latter is also intended to level the features associated with the finite interval of the transform. Depending on the function chosen, the visual pattern also changes, in particular, choosing the function could affect the resolution of the peaks in the distance.

Unfortunately, the resolution of the spectrometer described above does not allow identifying the distances those differ from each other by an amount less than 0.2 Å. In this connection, the coordination numbers are underestimated.

At the next stage, one performs a sequential verification of the remaining hypotheses. In order to do this, using the expected parameters of the coordination numbers, distances and the Debye–Waller factors, as well as the calculated amplitudes and phases a model function $\chi_{\mathrm{mod}}(k)$ is formed, which function is verified to correspond to the experimental one (see Fig. 6). The indicator of correspondence is usually presented by a matching factor (R), the average deviation (in percent). In the case of satisfactory coincidence (*i. e.* the consistency of the hypothesis) an iterative procedure is started that alters the expected parameters of the coordination numbers, distances, the Debye–Waller factors and E_0. In the course of this procedure, one obtains the exact values of these parameters for the sample under investigation. The iterative procedure is usually carried out in $\chi(k)$ space. From the basic formula

$$\chi(k) = \frac{1}{k}\sum_i \frac{N_i F_i(k)}{R_i^2} \exp(-2\sigma_i^2 k^2) \sin\left(2kR_i + \varphi_i(k)\right)$$

it follows that in the course of the iterative procedure the mentioned parameters could correlated between each other. To avoid this, the most of software products have visualizing the correlation matrix implemented.

In the case of putting forward and verifying the hypotheses, it should be taken into account that for the method of EXAFS, just as it is for the other methods that require the modelling of the experimental data, there is a limit concerning the number of independent parameters. The limit can be determined from the experimental data as

$$\eta = \frac{2}{\pi}\Delta R \Delta k + 2$$

where Δk is the interval of wave numbers, wherein the experimental data are modelled; ΔR is the interval of distances used in the Fourier filtering. In the case of exceeding the number of independent parameters, the results of simulation become ambiguous, thus different variants of the structure of the sample under investigation could result in the same matching factor value. In such a situation, it is often useful to neglect a part of structural information.

Verifying each hypothesis in terms of the deviation of the model function from the experimental one in most cases allows determining a level of matching the proposed local structure with respect to the real one.

APPLYING THE EXAFS TECHNIQUE TO STUDIES CONCERNING NANOMATERIALS

Using the method of EXAFS one can determine such physical parameters as interatomic distances from the atom whose absorption spectrum is registered, coordination numbers, interatomic distance deviation from the mean value (Debye–Waller factor). Measuring ranges for these values and determination errors are presented in Table 1. It should be noted that the EXAFS method has typical limitations inherent in X-ray based techniques: the distance to the light elements (hydrogen, lithium, beryllium, and boron, to some extent). The method allows determining the surroundings of the elements with atomic number, starting from $Z = 20$ (calcium). This limitation arises from the inability to register extended (not less than 600 eV) absorption spectra for the lighter elements without imposing the signals from the other electronic processes. In principle, the EXAFS method allows determining the atomic number of a chemical element located within the range of measured distances due to the peculiarities of the $F_i(k)$ function depending on the atomic number of the scattering element. However, the function itself is weakly dependent on the atomic number, so the error in the determination thereof is equal to ±4.

However, in many cases *via* EXAFS method one can determine the phase state of the object under investigation, the valence state, the structure of the first and several subsequent coordination spheres around the element under investigation. The main advantage of the method consists in the fact that the method allows determining these parameters also for X-ray amorphous systems, including solutions and objects *in vivo*. In addition, it can be used to establish the structure of the local environment for the majority of chemical elements contained in a complicated system under study, independently of each other. Using the SR additionally provides high measurement sensitivity and potentialities to investigate objects with the concentrations inaccessible to measure by means of laboratory instruments.

Determination of the phase state

Currently, many authors study the structure of ultrafine metal nanoparticles those are widely used in various fields of technology. They revealed the dependence of physical and chemical properties on the particle size [27]. A question arises whether the difference in the properties observed represents a consequence of the structural features of small particles with respect to bulk metal, or the main differences are caused by changing the morphology of the particles?

There are few works available from the literature whose authors registered significant structural differences between the metal particles synthesized at elevated temperature and the bulk metal [28, 29]. In contrast, small unsupported metal particles synthesized at a low temperature or metal films under strong interaction with the substrate demonstrated changing the crystallographic parameters and stabi-

lizing other crystalline modifications [30]. In the case of a high temperature reduction or surface interaction with the carrier or with reagents, structural relaxation is observed.

Even the metal nanoparticles produced by means of high temperature synthesis typically exhibit changes caused by the influence of the surface, which determines the differences in the surface and bulk structure of nanoparticles. So, single crystals exhibit the amplitude values of the thermal vibrations twice differ for the metal bulk and the surface [31]. Moreover, according to data from slow electron diffraction, in the case of single crystals the interplanar distances for the first skin layer can be different from the bulk of the crystal [32]. Similar effects could be expected for small particles, too, and, to all appearance, to a greater extent. However, the majority of the authors of papers devoted to the structure of metal nanoparticles do not report the influence of the surface. Whereas the structure of the metal particles is considered to be the same. Often, this is justified by the fact that the structural methods used in the study of small metal particles are sensitive to the particle bulk being insensitive to the surface. For such cases, one can check whether these differences are caused by a neglected surface contribution in the structural data. In this regard, of particular interest is catalyst EuroPt-1 that exhibits such a discrepancy to be known for long, with no explanation found yet. The program of developing a series of standard European catalysts, whose physicochemical properties should be extensively studied in various organizations, was launched in the late 1980ths, and the catalyst EuroPt-1 was the first in this series.

The standard platinum catalyst EuroPt-1 containing fine particles of platinum on SiO_2, is well studied. The review of studies devoted to this catalyst was presented by the authors of [33], whereas the composition and the surface structure of the catalyst were most completely described by the authors of [34, 35]. Owing to this, to analyze taking into account the surface influence upon the structure of nanoparticles, one suitably uses just the catalyst EuroPt-1. The authors of [34] *via* comparing experimental data and XRD profiles calculated according to the Debye formula determined that the original freshly prepared sample consists of cuboctahedral clusters containing 55 atoms of platinum. A part of platinum (36 % of total amount) is oxidized to be presented by the phase of platinum oxide PtO. Following the procedure of the dissolution of platinum ions by means of HCl/SnCl mixture, the authors of [36] revealed about 50 % of oxidized platinum. However, in determining the phase composition of the same sample by EXAFS spectroscopy the authors of [37–39] found that almost 90 % of Pt was oxidized. The authors of [40] in studying the reduced EuroPt-1 catalyst by means of EXAFS revealed that the entire platinum is only in the metallic state, but the values of coordination numbers for the shortest Pt–Pt distances are small (~5.5). Basing on this, the authors of [40] constructed a structural model of flat particles with a predominant (111) facet on the surface of platinum in the catalyst under consideration.

The investigation performed resulted in revealing [41] that some discrepancy between the data obtained from different methods is caused by structural distortions in the surface structure of small sized platinum clusters. However, the nature of such distortions is different for the original (oxidized) and reduced samples. So, in the case of the original sample the EXAFS data can be to the best described by a model wherein there are no differences in the values of Debye–Waller factor, but Pt–Pt distances in the bulk and on the surface differ from each other. On the contrary, in the case of reduced samples, a model is most likely wherein there are significant differences in the values of Debye–Waller factor for Pt–Pt distances in the bulk and on the surface, but the distances are comparable between each other.

There were numerous attempts in the literature to use EXAFS method for estimating the average size of nanoparticles [42], with no taking into account the above-mentioned peculiarities of the structure thereof.

The authors of the mentioned work calculated the number of atoms (N_{at}) in the platinum crystallite using the formula from [43]:

$$N_1 = a_1 N_{at}/(b_1 + N_{at}) + c_1 N_{at}/(d_1 + N_{at})$$

where N_1 is the coordination number for the first sphere; a_1, b_1, c_1 and d_1 are parameters taken from [43].

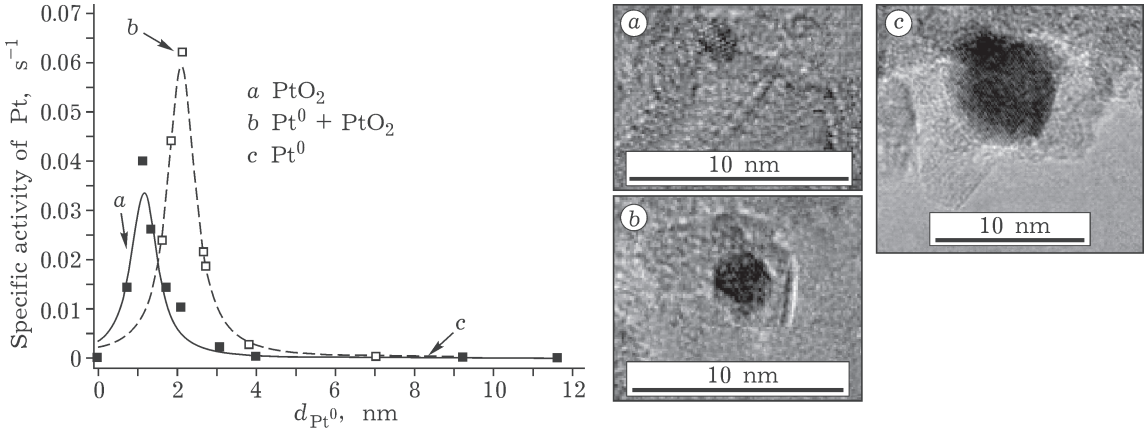

Fig. 8. Results of catalytic testing the oxidation of methanol and micrographs of platinum nanoparticles deposited onto Al_2O_3.

When calculating the size of the particles the authors based on the assumption that the crystallites of platinum have a hemispherical shape. The metal particle diameters determined in such a way amount to 16.5 and 19.5 Å for two different samples, respectively. It should be noted that owing to the features of the crystal structure of the metal particles within the hemisphere, these data might be unreliable. At the same time, these diameter values could be considered as the minimum allowable size of spherical particles.

In the course of determining the phase composition of a nanomaterial, the use of the coordination number inherent in the first interatomic distance metal–metal in order to estimate the fraction of a chemical element in the metallic state is unacceptable. However, just for this purpose one could use the value of the coordination number inherent in the metal–ligand distance for the elements with highly symmetric environment. These include the oxygen compounds of the most of chemical elements. For example, the authors of [44] basing on data concerning the coordination numbers performed phase analysis of a complex two-phase system with different methods of preparation (Figs. 8, 9).

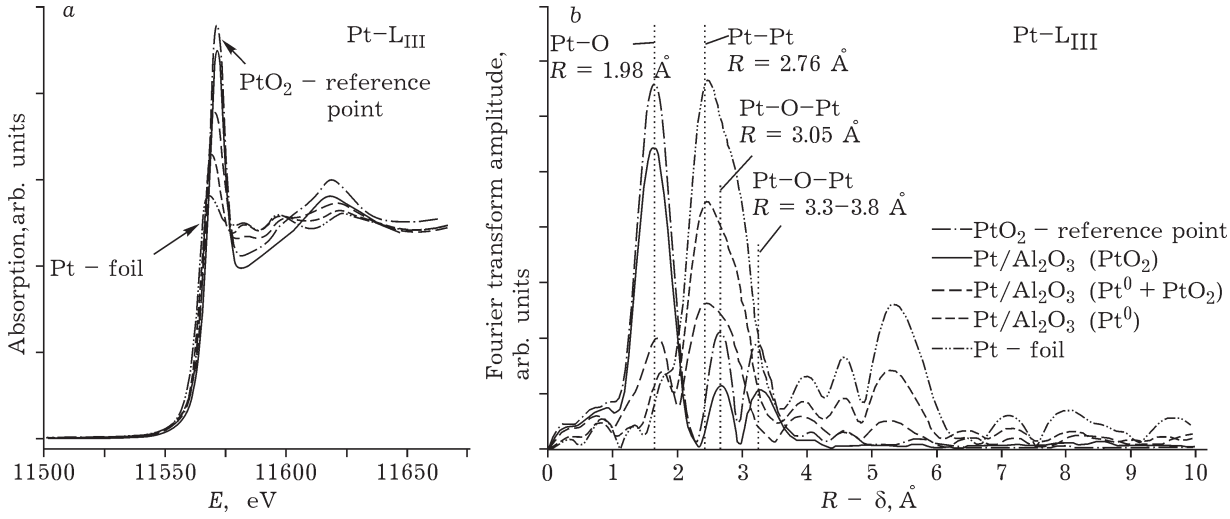

Fig. 9. XANES (*a*) and EXAFS (*b*) spectra of platinum nanoparticles applied onto Al_2O_3.

The authors of [45] performed the same analysis for a more complicated system consisting of gold nanoparticles attached to alumina modified with cerium and zirconium additives.

However, the role of EXAFS spectroscopy does not come to a statement of the presence and quantitative content of either phase. In the nanoscale state there could exist new metastable phases different from the phases those are stable in macroparticles or phases those are close to the phases inherent in bulk materials, but undergone any structural and electronic distortions.

The phases distorted owing to the nanoscale effects include, in particular, MoS_2 monolayer, consisting of a layer of S–Mo–S with the thickness less than 0.4 nm, but with a diameter equal to several tens of nanometres. Such MoS_2 undergoes significant structural changes. There is possibility of a structural transition of MoS_2 from the standard 2H modification (wherein the sulphur atoms form a trigonal prism around molybdenum) to 1T modification with an octahedral environment of molybdenum by sulphur [46]. Such an effect was observed, in particular, in the reaction between MoS_2 and hydrogen. Furthermore, there occurs shifting the molybdenum and sulphur atoms from their crystallographic positions. Depending on the degree of impact on MoS_2 through the basal plane and the magnitude of the charge transmitted thereto there are different structures formed. At a small value of the transmitted charge there occur superstructures of a charge-wave structure type with the displacements of atoms up to 0.1–0.2 Å [47] to form superstructures with a period of about 3 nm. In the case when the transferred charge value is large, a dimerization of molybdenum ions occurs with the formation of short bonds (about 2.8 Å), almost equal to the distances in Mo_2S_3. These effects persist up to 300 °C [48, 49] being connected with the fact that such systems are structurally unstable with respect to changing the electron density, including that caused by the interaction in the basal plane. In the course of adsorbing the reactants onto it or in the absence of the stabilizing influence of adjacent packages, a quasi-periodic superlattice occurs with a period of about 3 nm in the one-package catalyst. Each cluster in the superstructure represents a spherically curved MoS_2 package with changed Mo–S distances. Because of this, there occurs a set of shortest Mo–S and Mo–Mo distances, whose difference amounts to 0.007 nm. Such distortions can be studied only by means of EXAFS technique. Figure 10 presents the curves of RAD around molybdenum atoms for bulk and nanosized MoS_2. The scatter of Mo–S and Mo–Mo distances is exhibited by a decrease in the intensity of the first two peaks on the RAD curve. The distortion of the structure in the form of charge density waves are exhibited as a decrease in the intensity of the peak within the region of 0.6 nm [50].

The distortion of symmetry is exhibited in XANES spectra (Fig. 11).

Changing the shape of the absorption edge indicate the distortion in the symmetry of

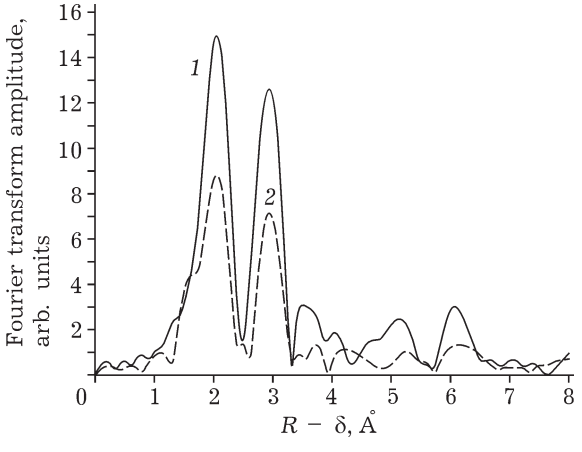

Fig. 10. Fourier transform modulus for the EXAFS spectra of supported catalysts MoS_2: *1* – MoS_2, *2* – MoS_2/Al_2O_3.

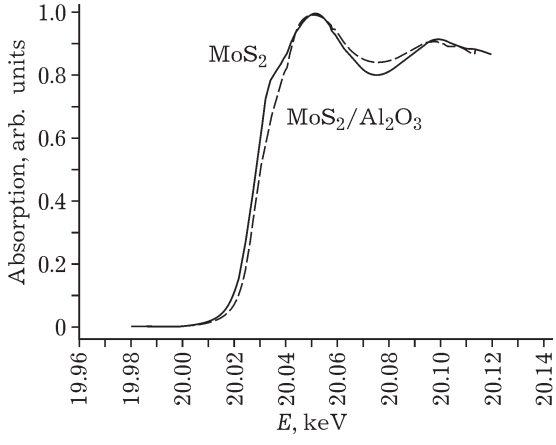

Fig. 11. XANES spectra of supported catalysts MoS_2.

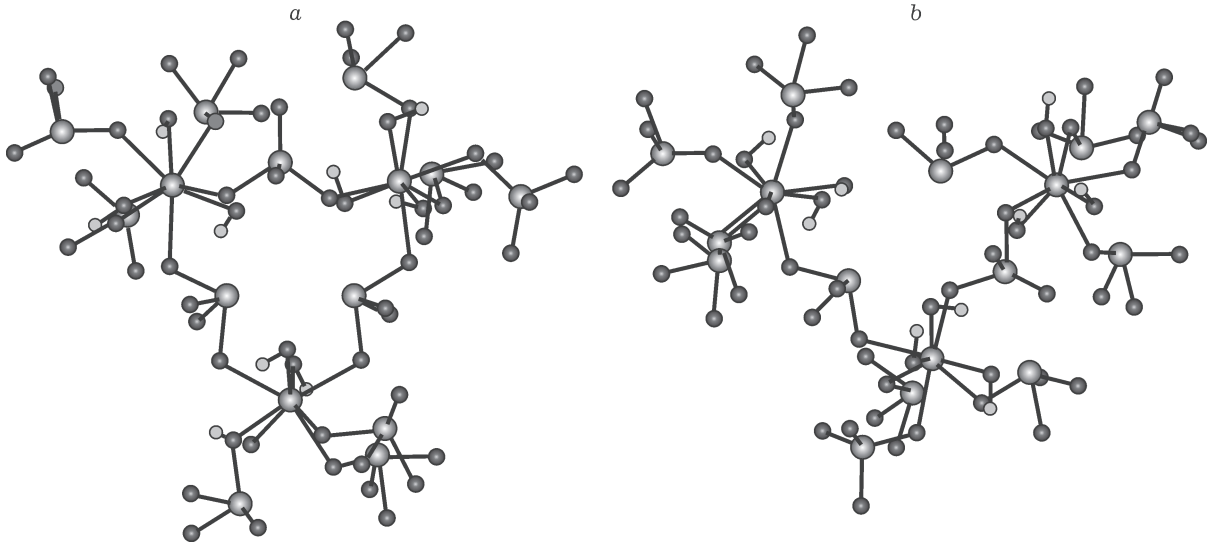

Fig. 12. Structure of closed (*a*) and open (*b*) zirconium oxychloride trimers in sulphuric acid solution.

molybdenum environment in nanosized MoS_2. More accurate data concerning the real symmetry of the molybdenum environment were obtained by means of Raman spectroscopy [51].

The determination of the phase composition of nanoparticles in solutions is also possible only with the use of the EXAFS method. So, before our studies [52, 53], it was thought that the solution of zirconium oxychloride in sulphuric acid could contain up to seven different zirconium compounds [54–56]. We demonstrated that in all the cases the zirconium is presented trimers those could be closed or opened (Fig. 12) depending on Zr/SO_4 ratio. The phases observed earlier were formed in the course of the transition of dissolved zirconium into the solid state, since the structure can be determined only for the solid phase.

Determination of the valence state

Figure 9, *a* demonstrates that the shape of the absorption edge of platinum depends on the valence state thereof. The feature observed is known as "white line" and the intensity thereof for 5*d* elements can be a base for determining the valence state of an element in nanoparticles, using reference compounds. The registration of chemical shift for the absorption edge of an element is considered as more com-

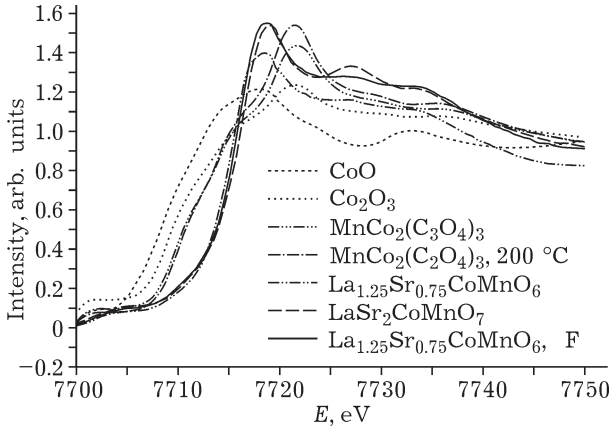

Fig. 13. XANES spectra of cobalt in different compounds.

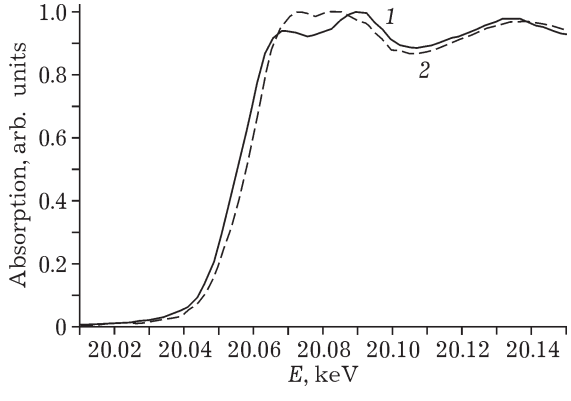

Fig. 14. XANES spectra of ruthenium depending on the presence of rubidium in the catalysts: *1* – without rubidium, *2* – with rubidium particles.

mon and applicable to the main type of atoms. The shift of the absorption edge towards a higher energy range indicates the occurrence and the value of the positive charge on the element under investigation. The magnitude of the shift depends on the valence state of the element and on the ligand environment thereof, *i. e.*, on the nature of the ligands, their number and the symmetry of the environment. Figure 13 demonstrates the absorption edge of cobalt depending on the valence state and the ligand environment thereof.

However, the shift of the absorption edge allows one to determine not only the valence state of the element in a nanoparticle, but also changing the charge state of nanoparticles without changing the valence, owing to the interaction with the carrier or chemisorption. So, Fig. 14 shows the XANES spectra of metallic ruthenium nanoparticles fixed on a carbon substrate, whose electronic properties are modified by the introduction of rubidium atoms. It is seen that ruthenium remains in the metal phase, but it obtains a positive charge, to all appearance, *via* the donation of a part of the electron density to the substrate.

CONCLUSION

Using the EXAFS and XANES methods with employing the synchrotron radiation often represents the only way to establish the local structure and the valence state of constituent chemical elements in the course of studying nanomaterials (often X-ray amorphous ones due to small size or because of the phase states) as well as substances with a low content of the chemical element under investigation.

With the help of EXAFS and XANES one could determine such characteristics of nanomaterials as the phase composition and the valence state of constituent chemical elements. Usually, to obtain such information researchers use the methods of X-ray diffraction, electron diffraction, transmission electron microscopy, and X-ray photoelectron spectroscopy to determine the valence state. Furthermore, methods are used those provide indirect information for determining the structural parameters. However, due to the fact that the mentioned methods exhibit some limitations in sensitivity and possibility of analyzing multi-element analysis of catalysts, they cannot be used for the investigation of multicomponent nanomaterials with the size of crystallized regions less than 10 nm and with the concentration element under investigation at less than 2–3 %. So, in this respect the methods of EXAFS and XANES currently have no alternative.

REFERENCES

1 Blokhin M. A., Fizika Rentgenovskikh Luchey, Gostekhizdat, Moscow, 1957.
2 Boroskiy I. B., Fizicheskiye Osnovy Rentgenospektralnykh Issledovaniy, Izd-vo MGU, Moscow, 1956.
3 Vainshteyn E. E., Rentgenovskiye Spektry Atomov v Molekulakh Khimicheskikh Soyedineniy i v Splavakh, Izd-vo AN SSSR, Moscow, 1950.
4 Kronig R. L. I., *Z. Phys.*, 70 (1931) 317.
5 Hayasi T., *Sci. Repts. Fohoku Univ. Ser. 1*, 33 (1943) 123.
6 Petersen H., *Z. Phys.*, 98 (1936) 569.
7 Hartree D. R., Kronig R. L., Petersen H., *Physica*, 1 (1934) 895.
8 Kostarev A. I., *Zh. Eksper. Teor. Phys.*, 2 (1941) 60.
9 Kostarev A. I., *Zh. Eksper. Teor. Phys.*, 19 (1949) 413.
10 Kozlenkov A. I., *Izv. AN SSSR. Ser. Fiz.*, 27 (1963) 364.
11 Kozlenkov A. I., *Izv. AN SSSR. Ser. Fiz.*, 25 (1963) 957.
12 Kozlenkov A. I., *Izv. AN SSSR. Ser. Fiz.*, 38 (1974) 500.
13 Sayers D. E., Lytle F. W., Stern E. A., *Adv. X-ray Anal.*, 13 (1970) 29.
14 Sayers D. E. A New Technique to Determine Amorphous Structure Using Extended X-ray Absorption Fine Structure (Ph. D. Thesises), University of Washington, Washington, 1971, p. 29.
15 Azaroff L. V., *Rev. Mod. Phys.*, 35 (1963) 1012.
16 Ashley C. A., Doniach S., *Phys. Rev. B*, 11 (1975) 1279.
17 Stern E. A., Heald S. M. Handbook on Synchrotron Radiation, North-Holland Publ. Co., Amsterdam, 1983, p. 955.
18 Parthasarathy R., Sarode P. R., Rao K. J., Rao C. N. R., *Proc. Indian Nat. Sci. Acad.*, 48A (1982) 119.
19 Kochubey D. I., Babanov Yu. A., Zamaraev K. I., Rentgenospektralny Metod Izucheniya Struktury Amorfnykh Tel: EXAFS-Spektroskopiaya, in G. M. Zhidomirov (Ed.), Nauka, Novosibirsk, 1988.
20 Schott G., Electromagnetic Radiation, Univ. Press, Cambridge, 1912.
21 Kulipanov G. N., Skrinskiy A. N., *Usp. Fiz. Nauk*, 122 (1977) 369.
22 X-Ray Data Booklet, Lawrence Berkeley Laboratory, Berkeley, 1985.
23 Kuper E. A., Ledenev A. V., *Avtometriya*, 4 (1978) 124.
24 Klementiev K. V., XAFSmass, April 2012, free-ware. URL: http://www.cells.es/Beamlines/CLAESS/software/xafsmass.html
25 FEFF code for ab inito calculations of XAFS – licensed software.
URL: http://leonardo.phys.washington.edu/feff/; a) Mustre de Leon J., Rehr J. J., Zabinsky S. I., Albers R. C., *Phys. Rev. B*, 44 (1991) 4146; b) Zabinsky S. I.,

Refr J. J., Ankudinov A. L., Albers R. C., Eller M. J., *Phys. Rev. B*, 52 (1995) 2995; c) Ankudinov A. L., Relativistic Spin-dependent X-ray Absorption Theory (Ph. D. Thesis), University of Washington, Washington, 1996.
26 Klementiev K. V., VIPER for Windows, freeware. URL: http://www.desy.de/~klmn/viper.html; Klementiev K. V., *J. Phys. D: Appl. Phys.*, 34 (2001) 209.
27 Beck I. E., Pakharukov I. V., Kriventsov V. V., Zaikovsky V. I., Nartova A. V., Parmon V. N., Bukhtiyarov V. I., Int. Symp. "Relations between Homogeneous and Heterogeneous Catalysis" (Abstracts), in G. A. Somorjai (Ed.), Univ. California, Berkeley, 2007, p. 91.
28 Moraweck B., Renouprez A. J., *Surf. Sci.*, 106 (1981) 35.
29 Moraweck B., Clugnet G., Renouprez A. J., *Surf. Sci.*, 81 (1979) L631.
30 Petrov Yu. I., Fizika Malykh Chastits, Nauka, Moscow, 1982.
31 Lyon H. B., Somorjai G. A., *J. Chem. Phys.*, 44 (1996) 3707.
32 Somorjaj G. A., *Catal. Lett.*, 7 (1990) 169.
33 Radivojevic D., Ruitenbeek M., Seshan K., Lefferts L., *J. Catal.*, 257 (2008) 255.
34 Kraynov A., Richards R., *Appl. Catal. A*, 314 (2006) 1.
35 Paal Z., Wootsch A., Schlogl R., Wild U., *Appl. Catal. A*, 282 (2005) 135.
36 Bond G. C., Paal Z., *Appl. Catal.*, 86 (1992) 11.
37 Gnutzman V., Vogel W., *J. Phys. Chem.*, 94 (1990) 4991.
38 Fulop E., Paal Z., Fogel W., *Appl. Catal.*, 66 (1990) 319.
39 Bond G. C., Wells P. B., *Appl. Catal.*, 18 (1985) 225.
40 Joyner R. W., *J. Chem. Soc. Faraday Trans. I*, 76 (1980) 357.
41 Moroz E. M., Kriventsov V. V., Kochubey D. I., *Zh. Struk. Khim.*, 50, 6 (2009) 1132.
42 Stakheev A. Yu., Tkachenko O. P., Klementyev K. V., Gryunert V., Bragina G. O., Mashkovskiy I. S., Kustov L. M., *Kinet. Katal.*, 46, 1 (2005) 114.
43 Jentys A., *Phys. Chem. Chem. Phys.*, 1 (1999) 4059.
44 Beck I. E., Bukhtiyarov V. I., Pakharukov I. Y., Zaikovsky V. I., Kriventsov V. V., Parmon V. N., *J. Catal.*, 268 (2009) 60.
45 Kriventsov V. V., Simakova I. L., Simakov A., Smolentseva E., Castillon F., Estrada M., Vargas E., Yakimchuk E, P., Ivanov D. P., Aksenov D. G., Andreev D. V., Novgorodov B. N., Kochubey D. I., Fuentes S., *Nucl. Instr. Meth.*, 603 (2009) 185.
46 Wypych F., Schoellhorn R. J., *Chem. Commun.*, (1992) 1386.
47 Schloellhorn R., *Chem. Mater.*, 8 (1996) 1747.
48 Rocquefelte X., Boucher F., Gressier P., Ouvrard G., Blaha P., and Schwarz K., *Phys. Rev. B*, 62 (2000) 2397.
49 Chu G. S., Bian G. Z., Fu Y. L., Zhang Z. C., *Mater Lett.*, 43 (2000) 81.
50 Kochubey D. I., Rogov V. A., Babenko V. P., *Kinet. Katal.*, 44 (2003) 135.
51 Kochubey D. I., Rogov V. A., Babenko V. P., *Reac. Kinet. Catal. Lett.*, 83, 1 (2004) 181.
52 Kanazhevskii V. V., Novgorodov B. N., Shmachkova V. P., Kotsarenko N. S., Kriventsov V. V., Kochubey D. I., *Mendeleev Commun.*, 6 (2001) 211.
53 Kanazhevskii V. V., Shmachkova V. P., Kotsarenko N. S., Kolomiychuk V. N., Kochubey D. I., *Zh. Struk. Khim.*, 47, 5 (2006) 876.
54 Nekhamkin L. G., Kolpachkova N. M., Kharitonova E. G., Kondrashova I. A., *Zh. Neorg. Khim.*, 27, 10 (1982) 2669.
55 Nekhamkin L. G., Tsylov Yu. A., Reznik A. M., *Izv. Vuzov. Tsv. Metallurgiya*, 2 (1984) 73.
56 Godneva M. M., Okhrimenko R. F., Kirichenko A. E., *Zh. Neorg. Khim.*, 31, 2 (1986) 360.